PCCP

PAPER

View Article Online
View Journal

On the thermodynamics of carbon nanotube single-file water loading: free energy, energy and entropy calculations†

Cite this: DOI: 10.1039/c3cp54554g

Jose Antonio Garate,[ab] Tomas Perez-Acle[ac] and Chris Oostenbrink*[a]

Received 28th October 2013,
Accepted 14th January 2014

DOI: 10.1039/c3cp54554g

www.rsc.org/pccp

Single-file water chains confined in carbon nanotubes have been extensively studied using molecular dynamics simulations. Specifically, the pore loading process of periodic (6,6) and (5,5) single-walled carbon nanotubes was thermodynamically characterized by means of free-energy calculations at every loading state and compared to bulk water employing thermodynamic cycles. Long simulations of each end-state allowed for the partitioning of the free energy into its energetic and entropic components. The calculations revealed that the initial loading states are dominated by entropic (both translational and rotational) components, whereas the latter stages are energetically driven by strong dipolar interactions among the water molecules in the file.

1 Introduction

Carbon Nanotubes (CNTs), due to their remarkable structural, mechanical and electromechanical properties,[1] have been revealed to be one of the most promising materials for building nanodevices in a large variety of applications, such as molecular detection,[2] membrane separation,[3] drug delivery, nanofluidic machines[4] and others. Moreover, at the theoretical level, CNTs are excellent systems for studying water confinement, allowing the modeling of complex structures such as water-permeable pores, which are ubiquitous in biological systems (*e.g.* membrane channels).[5] For these reasons, the characterization of the flux of water (and other fluids) through CNTs is of vital importance, permitting a clearer understanding of the mechanics in more complex biological media. Molecular Dynamics (MD) has proven to be an ideal tool for the aforementioned studies, and since the first work published dealing with MD simulation of water within CNTs,[6] other studies have followed it,[1,7–11] providing an improved picture of water dynamics within confined spaces.

Experimentally, water spontaneously fills the hydrophobic cavity of CNTs.[12–14] At the nanoscale level, the continuous description using hydrodynamics fails, as the flux is dominated by the movement of discrete particles; hence MD becomes the perfect method to describe the system at a particle level, allowing a detailed characterization of nanofluidics through CNTs, which can be extremely hard to attain using experimental means. One of the first studies demonstrated that water fills a (6,6) CNT spontaneously in a single-file fashion.[15,16] More recent studies employed different conditions such as pressure-driven water flux in hexagonal arrays of CNTs[8,17] or more realistic situations such as dipoles or charge distributions along the CNT, which are ubiquitous in biological systems.[9,18,19]

Many authors have described the thermodynamics of the water–CNT interactions. As the filling of the pores is a spontaneous phenomenon, the most common approaches for the estimation of free energies have been the calculations of Potentials of Mean of Force (PMF).[20] Other authors have used particle insertion strategies,[7,21,22] spectral analyses of velocity autocorrelation functions[23] and simple 1D-lattice models.[24] Overall, these studies indicate that the filling process is indeed a spontaneous process in spite of the hydrophobicity of the pore. For small tube diameters, the smooth walls force water molecules to form a highly ordered chain along the pore axis, the energetics of which is theoretically well understood. A strong electrostatic interaction is present due to the strong dipolar alignment[9,25] compensating for the loss of, on average, two hydrogen bonds. Additionally, the remaining hydrogen bond tends to be more directional and stable. On the other hand, entropic contributions have been more elusive, and despite extensive studies there is an ongoing debate on whether the filling process is entropically driven; recent reports present contradictory results on the magnitude and sign of the entropy of this transfer process.[21–23] Interestingly, some authors[23] have

[a] *Computational Biology Lab, Fundación Ciencia & Vida, Santiago, Chile. E-mail: jgarate@dlab.cl; Fax: +56 2 2372259; Tel: +56 2 3672000*
[b] *Institute for Molecular Modeling and Simulation, Muthgasse 18, Vienna, Austria. E-mail: chris.oostenbrink@boku.ac.at; Tel: +43 1 476548302*
[c] *Centro Interdisciplinario de Neurociencias de Valparaíiso, Universidad de Valparaíso, Pasaje Harrington 287, Playa Ancha, Valparaíso, Chile. E-mail: tomas@dlab.cl; Tel: +56 32 2508040*

† Electronic supplementary information (ESI) available. See DOI: 10.1039/c3cp54554g

reported that even for fully loaded tubes, entropy is the driving force and not only for the initial loading stages where the dipolar and dispersion interactions can hardly explain the spontaneous nature of this phenomenon.

To our knowledge, few studies have systematically studied the loading process,[21,22] and among these are the endeavors of Köfinger *et al.*[26] and Maibaum and Chandler[27] who have elegantly described the thermodynamics of single-file water through the use of lattice-models and Monte Carlo simulations. Remarkably, despite the simplicity of these models the main features of water enclosed in narrow pores are well described up to a macroscopic scale, including phenomena like proton defects and proton transport. Nevertheless, due to the nature (and beauty) of these simplified models entropic contributions are hard to attain and are estimated (optimized) by geometric considerations and included as parameters in the models.[26]

In this study we aim to fully describe the water-loading process with full atomistic simulations. Specifically, the free energy difference between all loading states was calculated, and both the energetic and entropic terms were computed. In detail, in analogy to biomolecular systems,[28] we considered the water molecules as the ''ligand'' whereas the CNT was taken as the ''receptor''. Accordingly, standard methods for studying binding free energies were employed, namely thermodynamic integration and thermodynamic cycling. For all these calculations, MD simulations of periodic (5,5) and (6,6) single-walled CNTs were employed, which are more representative of realistic tubes which have lengths on the order of tens of nanometers.[14] Additionally, the former avoids the intrinsic correlations that exist at the water–tube interface.[21] Moreover, long simulations at each loading state permitted the characterization of the energetic and entropic contributions, which could subsequently be rationalized in terms of hydrogen bonds, rotational relaxation times and diffusivity along the pore axis. We conclude that initial loading states are driven by entropy (both rotational and translational), with a gradual switch towards energetic contributions as the pore is filled up.

2 Methods

2.1 Thermodynamic integration

The free-energy difference (ΔA) between two states, A and B, can be readily calculated using the TI formula:

$$\Delta A_{\mathrm{A}\rightarrow\mathrm{B}} = \int_{\lambda=0}^{\lambda=1} \left\langle \frac{\partial \mathscr{V}(\lambda)}{\partial \lambda} \right\rangle_{\lambda} \mathrm{d}\lambda \qquad (1)$$

$\mathscr{V}(\lambda)$ is a combined potential energy function connecting the potential energy functions with a coupling parameter λ for states A ($\mathscr{V}_{\mathrm{A}}$ at λ = 0) and B ($\mathscr{V}_{\mathrm{B}}$ at λ = 1) respectively (see below). In the current setup, state A is represented by a SPC water molecule, while state B refers to a non-interacting dummy particle, devoid of any non-bonded interactions. In practice, $\left\langle \frac{\partial \mathscr{V}(\lambda)}{\partial \lambda} \right\rangle$ is computed at every λ point and then numerically integrated to obtain the free energy difference between states A and B.

An extra λ-dependent restraint to the perturbed water was employed, in order to maintain the particle that was being decoupled within the boundaries of a given region in space,

$$\mathscr{V}_{\mathrm{r}} = \frac{1}{2}\lambda K\left(r_{\mathrm{ij}}\right)^2 \qquad (2)$$

where K is the force constant for state B (λ = 1.0). The restraint was applied with respect to a neighboring water molecule in the file. In this way the dummy particle was confined within the tube, without altering the water flux through the tube axis. In some situations, a prefactor was utilized in eqn (2) to give

$$\mathscr{V}_{\mathrm{r}} = 2^{n+m}\lambda^n(1-\lambda)^m\frac{1}{2}\lambda K\left(r_{\mathrm{ij}}\right)^2 \qquad (3)$$

giving rise to the so called hidden restraints,[29] with user specified exponents n and m, with n = 2 and m = 0. This allows for both $\mathscr{V}_{\mathrm{r}}(\lambda)$ and $\frac{\partial \mathscr{V}_{\mathrm{r}}(\lambda)}{\partial \lambda}$ to be zero only at λ = 0.0.

2.2 Soft-core potential energy

A soft-core potential energy function[30] was employed to avoid singularities near the end-states of the TI simulations. The Lennard-Jones potential (LJ) energy function between atoms i and j at a state X is then defined as:

$$\mathscr{V}^{\mathrm{LJ}}\left(r_{\mathrm{ij}};\mathrm{X};\lambda\right) = \left[\frac{C_{12}^{\mathrm{X}}(\mathrm{i},\mathrm{j})}{\alpha_{\mathrm{LJ}}\lambda^2 C_{126}^{\mathrm{X}}(\mathrm{i},\mathrm{j}) + r_{\mathrm{i,j}}^6} - C_6^{\mathrm{X}}(\mathrm{i},\mathrm{j})\right]\cdot\frac{1}{\alpha_{\mathrm{LJ}}\lambda^2 C_{126}^{\mathrm{X}}(\mathrm{i},\mathrm{j}) + r_{\mathrm{i,j}}^6} \qquad (4)$$

α_{LJ} is the softness parameter for the LJ interaction and $r_{\mathrm{i,j}}$ the distance between atoms i and j. $C_{12}^{\mathrm{X}}(\mathrm{i},\mathrm{j})$ and $C_6^{\mathrm{X}}(\mathrm{i},\mathrm{j})$ are the r^{12} and r^6 LJ parameters for the atom pair (i,j). $C_{126}^{\mathrm{X}}(\mathrm{i},\mathrm{j})$ equals $C_{12}^{\mathrm{X}}(\mathrm{i},\mathrm{j})/C_6^{\mathrm{X}}(\mathrm{i},\mathrm{j})$ when $C_6^{\mathrm{X}}(\mathrm{i},\mathrm{j}) \neq 0$ and zero otherwise. Likewise, the electrostatic interaction with the soft-core potential energy function becomes:

$$\mathscr{V}^{\mathrm{CRF}}\left(r_{\mathrm{ij}};\mathrm{X};\lambda\right) = \frac{q_{\mathrm{i}}^{\mathrm{X}}q_{\mathrm{i}}^{\mathrm{X}}}{4\pi\varepsilon_0\varepsilon_1}\left[\frac{1}{\left[\alpha_{\mathrm{CRF}}(\mathrm{i},\mathrm{j})\lambda^2 + r_{\mathrm{i,j}}^2\right]^{\frac{1}{2}}} - \frac{\frac{1}{2}C_{\mathrm{rf}}r_{\mathrm{i,j}}^2}{\left[\alpha_{\mathrm{CRF}}(\mathrm{i},\mathrm{j})\lambda^2 + R_{\mathrm{rf}}^2\right]^{\frac{3}{2}}} - \frac{\left(1-\frac{1}{2}C_{\mathrm{rf}}\right)}{R_{\mathrm{rf}}}\right] \qquad (5)$$

$q_{\mathrm{i}}^{\mathrm{X}}$ is the partial charge of atom i and C_{rf} and R_{rf} are parameters of the reaction-field method. α_{CRF} is the softness parameter for the electrostatic interactions.

The total nonbonded potential energy for atoms i,j in a given state is calculated as:

$$\mathscr{V}^{\mathrm{NB}}(r_{\mathrm{ij}};\mathrm{X};\lambda) = \mathscr{V}^{\mathrm{LJ}}(r_{\mathrm{ij}};\mathrm{X};\lambda) + \mathscr{V}^{\mathrm{CRF}}(r_{\mathrm{ij}};\mathrm{X};\lambda) \qquad (6)$$

The combined non-bonded potential energy function connecting states A and B is now:

$$\mathscr{V}^{\mathrm{NB}}(r_{\mathrm{ij}};\lambda) = \lambda\mathscr{V}^{\mathrm{NB}}(r_{\mathrm{i,j}};\mathrm{B};(1-\lambda)) + (1-\lambda)\mathscr{V}^{\mathrm{NB}}(r_{\mathrm{i,j}};\mathrm{A};\lambda) \qquad (7)$$

2.3 Free energy of transfer

Consider two systems, one of N bulk water molecules in a volume V (N system) and one of n water molecules in a tube solvated in a box of water in the same volume V (n system). $\mathcal{N}$ atoms make up the tube and the solvating water molecules in the latter system. The combined canonical partition function is:

$$Q_{(N,n,\mathcal{N},V,T)} = \frac{C}{n!\cdot\mathcal{N}!\cdot N!}\int_V \mathrm{d}q^N \int_V \mathrm{d}q^{\mathcal{N}}\cdot\mathrm{d}q^n\cdot \mathrm{e}^{-\beta\mathscr{V}_{(N,n,\mathcal{N})}} \quad (8)$$

where $\mathscr{V}_{(N,n,\mathcal{N})} = \mathscr{V}_N + \mathscr{V}_n$, with $\mathscr{V}_N$ and $\mathscr{V}_n$ being the potential energies of the N and n systems respectively. $\beta = 1/k_BT$, with k_B the Boltzmann constant, T the temperature and C a constant. Similarly, the combined partition function of a box with $N-1$ water molecules of volume V ($N-1$ system) and a tube with $n+1$ water molecules within the pore embedded in a box with water of the same volume V ($n+1$ system), is:

$$Q_{(N-1,n+1,\mathcal{N},V,T)} = \frac{C}{(n+1)!\cdot\mathcal{N}!\cdot(N-1)!}\int_V \mathrm{d}q^{N-1}\cdot\int_V \mathrm{d}q^{\mathcal{N}}\cdot\mathrm{d}q^{n+1}\cdot \mathrm{e}^{-\beta\mathscr{V}_{(N-1,n+1,\mathcal{N})}} \quad (9)$$

with $\mathscr{V}_{(n+1,N-1)} = \mathscr{V}_{N-1} + \mathscr{V}_{n+1}$, where $\mathscr{V}_{N-1}$ and $\mathscr{V}_{n+1}$ are the potential energies with the $N-1$ and $n+1$ systems, respectively. Given that $\mathscr{V}_N$ (or $\mathscr{V}_{N-1}$) and $\mathscr{V}_n$ (or $\mathscr{V}_{n+1}$) are uncorrelated. In other words, as the specific configurations of the solvent do not alter the interactions of the loaded particles, we can write the following:

$$Q_{(N,n,\mathcal{N},V,T)} = \frac{C}{n!\cdot\mathcal{N}!\cdot N!}\int_V \mathrm{d}q^N\cdot\mathrm{e}^{-\beta\mathscr{V}_N} \times\int_V \mathrm{d}q^{\mathcal{N}}\cdot\mathrm{d}q^n\cdot\mathrm{e}^{-\beta\mathscr{V}_n} \quad (10)$$

$$Q_{(N-1,n+1,\mathcal{N},V,T)} = \frac{C}{(n+1)!\cdot\mathcal{N}!\cdot(N-1)!}\int_V \mathrm{d}q^{N-1}\cdot\mathrm{e}^{-\beta\mathscr{V}_{N-1}} \times\int_V \mathrm{d}q^{\mathcal{N}}\cdot\mathrm{d}q^{n+1}\cdot\mathrm{e}^{-\beta\mathscr{V}_{n+1}} \quad (11)$$

The free energy (ΔA) of transferring a water molecule from the pore to the bulk is directly related to the quotient between eqn (10) and (11):

$$\Delta A_{(n+1,N-1)\to(n,N)} = -k_BT\ln\frac{Q_{(N,n,\mathcal{N},V,T)}}{Q_{(N-1,n+1,\mathcal{N},V,T)}} \quad (12)$$

$$\frac{Q_{(N,n,\mathcal{N},V,T)}}{Q_{(N-1,n+1,\mathcal{N},V,T)}} = \frac{n+1}{N}\cdot\frac{\int_V \mathrm{d}q^N\cdot\mathrm{d}q^n\cdot\mathrm{e}^{-\beta\mathscr{V}_N}\int_V \mathrm{d}q^{\mathcal{N}}\cdot\mathrm{e}^{-\beta\mathscr{V}_n}}{\int_V \mathrm{d}q^{N-1}\cdot\mathrm{e}^{-\beta\mathscr{V}_{N-1}}\int_V \mathrm{d}q^{\mathcal{N}}\cdot\mathrm{d}q^{n+1}\cdot\mathrm{e}^{-\beta\mathscr{V}_{n+1}}} \quad (13)$$

Employing Zwanzig's formula,[31] we can write this quotient as:

$$\frac{Q_{(N,n,\mathcal{N},V,T)}}{Q_{(N-1,n+1,\mathcal{N},V,T)}} = \frac{n+1}{N}\cdot\frac{\left\langle \mathrm{e}^{-\beta(\mathscr{V}_n-\mathscr{V}_{n+1})}\right\rangle_{n+1}}{\left\langle \mathrm{e}^{-\beta(\mathscr{V}_{N-1}-\mathscr{V}_N)}\right\rangle_N} \quad (14)$$

where the triangular brackets denote an ensemble average over a simulation run for state $n+1$ or N. Applying eqn (12):

$$\begin{aligned}\Delta A_{(n+1,N-1)\to(n,N)} &= \Delta A_{\mathrm{transfer}}\\ &= -k_BT\ln\left(\frac{n+1}{N}\right) - k_BT\ln\left\langle \mathrm{e}^{-\beta(\mathscr{V}_n-\mathscr{V}_{n+1})}\right\rangle_{n+1}\\ &\quad + k_BT\ln\left\langle \mathrm{e}^{-\beta(\mathscr{V}_{N-1}-\mathscr{V}_N)}\right\rangle_N\\ &= \Delta A_1 + \Delta A_2 - \Delta A_3 \end{aligned} \quad (15)$$

The first term of eqn (15) is a correction due to the indistinguishability of the particles "binding" to the tube. In the case of one ligand being transfered from infinite dilution to a single site, this correction equals zero. The second term accounts for the alchemical decoupling of a water molecule within the pore. To avoid the "wandering-ligand" problem, a harmonic potential energy function is applied to restrain the dummy particle within the cavity. ΔA_2 can be decomposed into an alchemical term (which includes the contribution of the harmonic potential energy, eqn (2)) plus the transfer of a restrained dummy to the bulk, *i.e.* removal of restraints:

$$\Delta A_2 = \Delta A_{2A} + \Delta A_{2T} \quad (16)$$

$$\Delta A_{2T} = -k_BT\ln\frac{V}{\left(\frac{2\pi k_BT}{K}\right)^{\frac{3}{2}}} \quad (17)$$

where V is the volume of the system and K is the force constant of the harmonic oscillator. Similarly, the third term of (15) equals the decoupling of a water molecule in the bulk phase, which is equivalent to the water–water desolvation free energy; ΔA_3 and ΔA_{2A} are computed employing eqn (1), whereas ΔA_1 and ΔA_{2T} are computed analytically, not requiring further simulations. In Fig. 1, the thermodynamic cycle depicting the unloading process is shown.

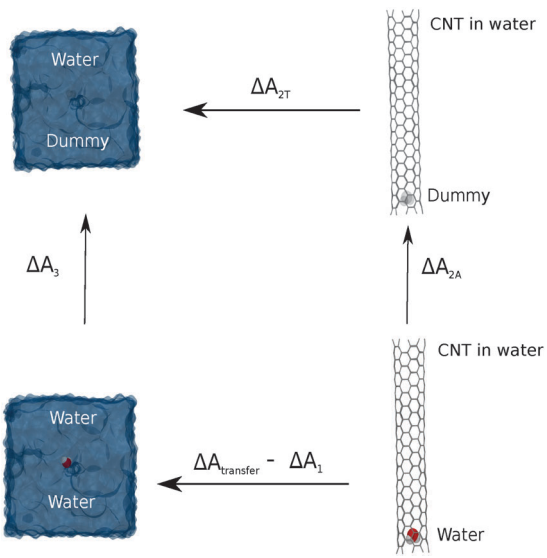

Fig. 1 Proposed thermodynamic cycle for the free energy of unloading the CNT. The individual free energy terms are defined in eqn (15)–(18).

Imposing that $\mathcal{V}_N$ (or $\mathcal{V}_{N-1}$) and $\mathcal{V}_n$ (or $\mathcal{V}_{n+1}$) are uncorrelated, in other words the specific configurations of the bulk do not influence the water molecules within the tube and *vice versa*, we can compare the previous derivation with PMF calculations from simulations of open (finite) tubes:

$$\mathrm{PMF}_{(n+1,N-1)\rightarrow(n,N)} = -k_\mathrm{B}T\ln\left(\frac{P_{n-1}}{P_n}\right) \quad (18)$$

where P_{n-1} and P_n are the probabilities of finding $n-1$ or n molecules inside the tube, respectively. An equivalent derivation was carried out employing a grand canonical formalism[9,21] or thermodynamic cycling.[28]

2.4 Entropy of transfer

Entropy was calculated from the total energy by:

$$T\Delta S_\mathrm{transfer} = \Delta\langle E\rangle - \Delta A_\mathrm{transfer} \quad (19)$$

where $\Delta\langle E\rangle$ is the difference between the average energy of two loading states increased by the average solvation energy of water in the bulk.[32]

2.5 Average loading from free energies

Average loadings were computed by weighting each loading state ($\mathcal{N}$) with its corresponding free energy employing the following expression:

$$\langle\mathcal{N}\rangle = \sum_{\mathcal{N}=0}^{\mathrm{ML}} \mathcal{N}\mathrm{e}^{\frac{-\Delta A_\mathcal{N}}{k_\mathrm{B}T}} \quad (20)$$

where $\Delta A_\mathcal{N} = \sum_{n=0}^{n=\mathcal{N}} \Delta A_{(n,N)\rightarrow(n+1,N-1)}$; in other words, the cumulative transfer free energies (see eqn (15)) up to the loading state $\mathcal{N}$. ML represents the maximum loading state simulated.

2.6 Rotational relaxation

Reorientation correlation functions $C_\alpha(t)$ of SPC water were computed for the dipole (μ) and the H–H vectors,

$$C_\alpha(t) = \langle\mathbf{e}_\alpha(t)\cdot\mathbf{e}_\alpha(0)\rangle \quad (21)$$

where $\mathbf{e}_\alpha$ is a unit vector pointing along the direction of the α axis. $C_\alpha(t)$ normally shows an exponential decay, and can be fitted employing the following expression:

$$C_\alpha(t) = A\exp\left(\frac{-t}{\tau_\alpha}\right) \quad (22)$$

τ_α denotes the first-order rotational relaxation time and A is a constant.

2.7 Water self-diffusion

Self-diffusion coefficients along the pore axis (D_z) for the oxygen of SPC water were calculated from mean-squared displacements (MSD), using the Einstein relation:[33]

$$D_z = \lim_{t\rightarrow\infty}\frac{\left\langle\left(r_z(t_0+t)-r_z(t_0)\right)^2\right\rangle_{t_0}}{2t} \quad (23)$$

where $r_z(t)$ corresponds to the z component of the oxygen position vector at time t, and the averaging is performed over multiple time origins (t_0) and water molecules.

2.8 Molecular dynamics simulations

All MD simulations were performed using the GROMOS11 simulation package.[34,35] The SHAKE algorithm[36] was employed to constrain all bonds and water angles to their reference values with a relative tolerance of 10^{-4}, allowing for a time-step of 2 fs using the leapfrog algorithm.[37] Periodic boundary conditions with a rectangular box were applied. Non-bonded interactions were computed using a triple range cut-off. Interactions within a short-range cut-off of 0.8 nm were computed for every time-step, from a pair-list that was generated every 5 steps. At these time points, interactions between 0.8 and 1.4 nm were also computed and kept constant between updates. A reaction-field contribution was added to coulombic interactions approximating a homogeneous medium outside the long-range cut-off, employing the relative permittivity of SPC water (61).[38] All interactions were calculated using the GROMOS 45A4 parameter set; specifically all CNT atoms were modelled as sp^2 carbons.[39] After a steepest-descent minimization to remove bad contacts, velocities were randomly assigned from a Maxwell–Boltzmann distribution at 298 K. All simulations were run at the canonical (NVT) ensemble using the Nosé–Hoover chains coupling algorithm for temperature (3 chains, 298 K).[40,41] The solute and solvent atoms were independently coupled to the heat bath. Due to a decoupling of translations and rotations within the periodic tubes, these were thermostated independently. Periodic (6,6) and (5,5) tubes along the z-axis of length 3.19 nm and widths 0.80 and 0.68 nm respectively, were placed in a rectangular box of size $3.6\times3.6\times3.19$ nm^3 comprising a total number of 4047 atoms for the (6,6) system and 4094 atoms for the (5,5) system. A depiction of the simulated system is shown in Fig. 2.

In detail, 13 water molecules were placed within the pores and were sequentially removed. For this purpose, TI simulations were performed for SPC water annihilation, which on average, encompassed 17 non-equidistant windows and 1.5 ns

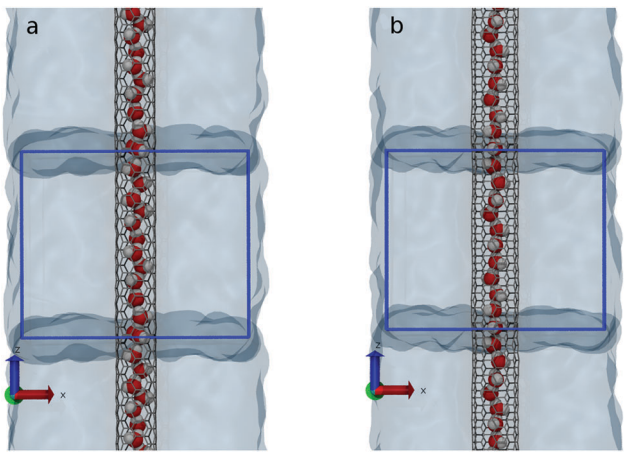

Fig. 2 Simulated systems, the periodic cell is depicted in blue. (a) (5,5) single-walled CNT system. (b) (6,6) single-walled CNT system.

of simulation time per window. Calculations were conducted using a non-bonded soft-core potential energy function[30] with softness parameters $\alpha_{LJ} = 0.5$ and $\alpha_{CRF} = 0.5$ nm^2. Given that the free energy is a state function, the specific values of these parameters should not affect the final ΔA calculated with eqn (1). Previous work by de Ruiter *et al.* has shown that the chosen parameters deviate less than k_BT from a set of reference simulations.[42] Each loading state (from 13 to 0 water molecules) was also simulated for 100 ns, in order to obtain converged energies for use in eqn (19). Moreover, due to the short relaxation times of the H–H vector (see eqn (21) and (22)) extra 1 ns simulations for each loading state, saving coordinates every 10 fs were carried out. Lastly, and for comparison, free simulations of bulk SPC (40 ns) and open non-periodic (6,6) and (5,5) single-walled CNTs were conducted for 20 ns and 100 ns respectively using the same length of the CNTs and a box size of 4.8 × 4.8 × 4.8 nm^3. Overall, the total simulation time amounted to 3.38 μs.

3 Results and discussion

3.1 Transfer free energies, energies and entropies

In Table 1, $\Delta A_{transfer}$, $\Delta E_{transfer}$ and $T\Delta S_{transfer}$ employing eqn (15) and (19) are presented. A summary of the TI simulations and convergence analyses for total potential energies can be found in ESI† (see Fig. S1–S4 and Table S1). A fully loaded tube was defined by the maximum loading state recorded in free open-tube simulations, which was 13 and 11 water molecules for the (6,6) and (5,5) systems, respectively.

3.2 Transfer free energies

Transfer free energies ($\Delta A_{(n+1)\rightarrow(n)}$) for the (6,6) and (5,5) systems are presented in Table 1. $\Delta A^{(6,6)}_{(n+1)\rightarrow(n)}$ is always favorable towards the confined conditions, including the case for $n = 1$. The deeper free energies for the fully loaded states ($n > 10$) are a direct consequence of enhanced electrostatics due to periodicity.

The (5,5) system, on the other hand, favors the unloaded states. Only for high loadings are the electrostatic interactions able to fully compensate the strong confinement, rendering $\Delta A^{(5,5)}_{(11)\rightarrow(10)}$ positive. It is important to notice the low values for the energetic and entropic components which are, in general, always within k_BT, implying a big uncertainty in these free energies due to typical thermal fluctuations. The latter suggests a bimodal mode, where the tube is either empty or filled. For an open tube, other authors have shown this behavior.[7,21,22]

3.2.1 Cumulative transfer free energies. With the aim of having a full picture of the loading process, cumulative free energies for the loading process (and its energetic and entropic components) are depicted in Fig. 3. Additionally, results from cumulative PMF calculations of open non-periodic tubes employing eqn (18) are included. In the case of the (6,6) free simulations, below loadings of $n = 8$, no events were recorded; thus it was assumed that the cumulative free energies were equivalent up to that point. For more details on the open non-periodic tube's PMFs, refer to Fig. S5 (ESI†).

Regarding the (6,6) system, the total ΔA, ΔE and $T\Delta S$ of loading 12 water molecules (which is the most favorable loading)

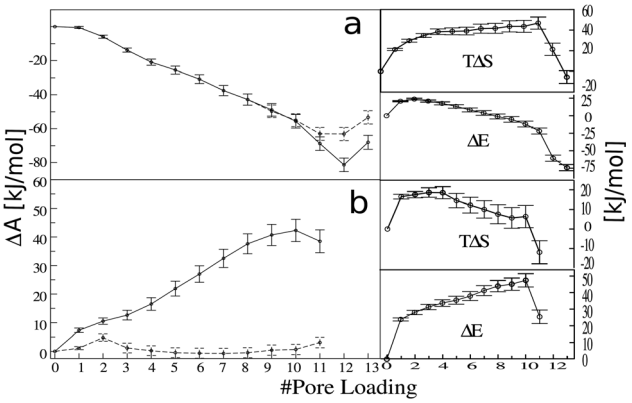

Fig. 3 Cumulative transfer free energies from the bulk ($\Delta A_{transfer}$) for the (6,6) system (panel a) and (5,5) system (panel b). Dashed lines depict the cumulative free energies for the open non-periodic systems. The panels on the right show the cumulative entropies and energies of transfer from the bulk.

Table 1 $\Delta A_{(n+1,N-1)\rightarrow(n,N)}$, $\Delta E_{(n+1,N-1)\rightarrow(n,N)}$ and $T\Delta S_{(n+1,N-1)\rightarrow(n,N)}$ in kJ mol^{-1} for the (6,6) and (5,5) single-walled CNT systems[a]

	System (6,6)			System (5,5)		
# Pore loading transition	ΔA	ΔE	$T\Delta S$	ΔA	ΔE	$T\Delta S$
13 → 12	−13.3 ± 0.7	13.5 ± 0.8	26.8 ± 1.1	−169.0 ± 1.6	−126.4 ± 0.8	42.6 ± 1.8
12 → 11	12.5 ± 0.6	38.0 ± 0.8	25.5 ± 1.0	−37.2 ± 0.9	−5.5 ± 0.9	31.8 ± 1.2
11 → 10	13.2 ± 0.7	10.0 ± 0.8	−3.2 ± 1.1	3.8 ± 0.8	22.0 ± 0.9	18.2 ± 1.1
10 → 9	6.7 ± 1.4	6.7 ± 1.5	0.0 ± 2.1	−1.6 ± 1.1	−2.3 ± 1.1	−0.7 ± 1.5
9 → 8	6.1 ± 1.7	4.1 ±1.7	−1.9 ± 2.4	−3.1 ± 1.4	−1.2 ± 1.5	1.9 ± 2.1
8 → 7	5.3 ± 1.3	5.0 ± 1.4	−0.3 ± 1.9	−5.1 ± 1.4	−2.7 ± 1.5	2.4 ± 2.1
7 → 6	6.7 ± 1.6[b]	4.4 ± 1.7	−2.3 ± 2.4	−5.5 ± 1.4[b]	−3.3 ± 1.4	2.2 ± 1.9
6 → 5	5.3 ± 1.2[b]	5.0 ± 1.3	−0.3 ± 1.7	−5.1 ± 1.2[b]	−2.5 ± 1.2	2.7 ± 1.7
5 → 4	4.6 ± 1.4	4.3 ± 1.4	−0.4 ± 2.0	−5.4 ± 1.3[b]	−1.7 ± 1.3	3.6 ± 1.8
4 → 3	7.1 ± 1.3	3.3 ± 1.4	−3.7 ± 1.9	−3.9 ± 1.4[b]	−2.4 ± 1.5	1.5 ± 2.0
3 → 2	7.9 ± 0.8	2.9 ± 0.9	−5.0 ± 1.2	−2.1 ± 1.3	−3.3 ± 1.3	−1.1 ± 1.8
2 → 1	5.4 ± 0.7	−3.1 ± 0.8	−8.5 ± 1.0	−3.2 ± 0.8	−4.2 ± 0.9	−1.0 ± 1.3
1 → 0	0.5 ± 0.6	−20.7 ± 0.8	−21.2 ± 1.0	−7.3 ± 0.8	−23.8 ± 0.9	−16.5 ± 1.2
Bulk SPC	25.9 ± 0.4	44.9 ± 0.4	19.0 ± 0.6	—	—	—

[a] Errors are obtained by calculating block averages, extrapolating to infinite block length. [b] Eqn (3) was used instead of (2) to reduce the noise at $\lambda = 0$.

amounted to −82.0, −60.7 and 21.3 kJ mol^{-1}, respectively. Therefore, the full process is both entropically and energetically driven. From the triple panels of Fig. 3 two phases for the loading process can be characterized: an entropically driven stage at low loadings and an energetically driven phase at high loadings. With respect to the PMF calculations, a similar trend is observed, the shift to higher ΔA's can be credited to the lack of periodicity and the intrinsic differences between the simulated systems *i.e.* water–tube interface correlations. Specifically, at high loadings, the dipolar coupling between the water molecules within the pore expands across the periodic boundaries; in fact, an extra hydrogen bond is formed between periodic images of the water file. Due to the purely energetic contribution of this extra interaction, the more favourable values of ΔA for the periodic system at these loading stages (mainly energetically driven) are expected. Employing the ΔA values of Fig. 3 in eqn (20) rendered an average loading of 11.98 water molecules which is in good agreement with the average loading of 11.78 observed for open simulations.

For the (5,5) systems, the differences between the open and the periodic tubes are significant. While the cumulative ΔA values from the periodic system show a continuous increase up to pore loadings of n = 10, the cumulative PMF from the open systems is relatively flat with values around 0 kJ mol^{-1}. In this simulation a bimodal mode pore loading switching between completely filled and completely empty was observed and the loading distributions were essentially equal at simulation times of 25, 50 and 100 ns. Similar simulations at constant pressure favored the fully loaded state (data not shown), suggesting that this system is more sensitive to the pressure and the presence of a vacuum within the tube. This means that our initial assumption that the water configurations in the bulk are largely uncorrelated with the waters in the tube does not hold and a comparison between the periodic and non-periodic systems becomes meaningless. For the periodic systems, loading the tube up to 11 water molecules is unfavorable with ΔA, ΔE and $T\Delta S$ amounting to 37.3, 25.4 and −11.9 kJ mol^{-1}, respectively.

3.3 Transfer energies

Energy contributions are proportional to the amount of water molecules located within the cavity; at initial loading stages, negative $\Delta E^{(6,6)}_{(n+1)\rightarrow(n)}$ are observed. This is expected as van der Waals interactions between the pore atoms and a single water molecule cannot compensate for the dipolar and hydrogen bond interactions of the bulk. This energetic gain is not as severe compared to the heat of solvation of water (ΔE^{solv} = −44.9 kJ mol^{-1}), implying that the pore only partially decouples the water molecule from the bulk. The reported values for infinite pores are in line with our calculations.[21] Periodicity effects are present, which are reflected in the considerably higher values of $\Delta E^{(6,6)}_{(1)\rightarrow(0)}$ = −6.8 kJ mol^{-1} previously reported for open tubes.[22] This can be explained by correlations of this single water molecule with the bulk phase in open systems. From 23% of loading, $\Delta E^{(6,6)}_{(n+1)\rightarrow(n)}$ increasingly favors the confined state, with an average constant rate of 4.5 kJ mol^{-1} per added water molecule. At loadings larger than 84%, the energy experiences a dramatic jump; in these states water is tightly packed forming an unruptured chain which enhances dipolar and hydrogen bond interactions. Moreover, periodicity effects are also present, with the water chain now forming an extra H-bond with its periodic image.

Energetically the (5,5) system shows a peculiar trend. As in the (6,6) system, initially a negative $\Delta E^{(5,5)}_{(1)\rightarrow(0)}$ is observed, which is maintained up to 90% of loading. The energetic differences are very small and within $k_{\mathrm{B}}T$. At n = 11, this trend notably shifts toward a positive value, which again is due to periodicity effects as an additional H-bond can be formed. Further loadings are strongly unfavorable towards the confined state.

3.3.1 Water-file energy components. Other authors have described single-file water solely in terms of water–water interactions.[26,27] To explore the validity of this approach we investigated the specific energetics of the single water chain for loaded states. In detail, the non-bonded interaction energies of the water file were decomposed into 3 terms: water-file–tube (WF–T), water-file–solvent (WF–S) and water-file–water-file (WF–WF) interactions, these three terms were subsequently decomposed into their van der Waals and Coulombic components, for a total of 5 terms (the CNT atoms have zero partial charges). Fig. 4 presents normalized $\langle E_{\mathrm{WF-T}}\rangle$, $\langle E_{\mathrm{WF-S}}\rangle$ and $\langle E_{\mathrm{WF-WF}}\rangle$ as functions of pore loadings. Intrinsically, the interactions between the water file and the surroundings are almost independent of the loading ($\langle E^{6,6}_{\mathrm{WF-T}}\rangle \approx -22$ kJ mol^{-1}, $\langle E^{5,5}_{\mathrm{WF-T}}\rangle \approx -19$ kJ mol^{-1}). The same occurs for $\langle E_{\mathrm{WF-S}}\rangle \approx -2$ kJ mol^{-1} for all loadings, therefore these interactions could be added as parameters in more simplified models as effective chemical

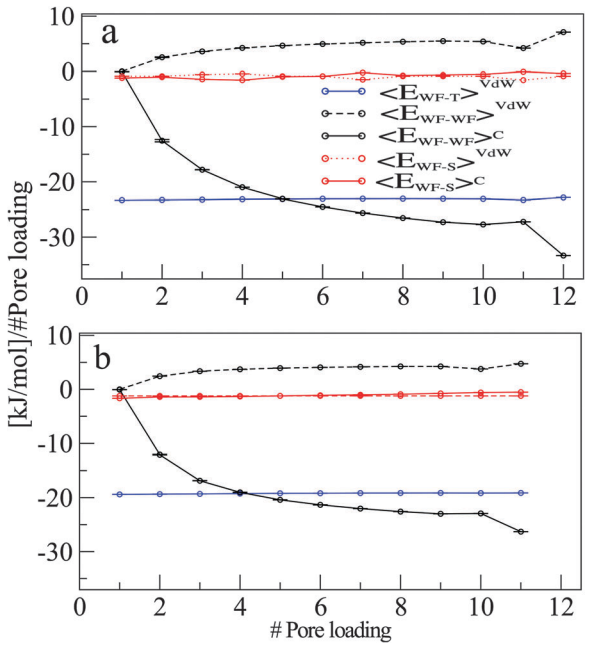

Fig. 4 Normalized non-bonded interaction energies (E) for the water file components as a function of each loading state for the (6,6) system (panel a), and (5,5) system (panel b). WF–T: water-file tube; WF–WF water-file water-file interaction energy; WF–S water-file solvent interaction energy. VdW: van der Waals; C: Coulomb.

potentials.[27] Moreover, the solvent could be treated as continuous, supporting the previous assumption of no correlations among configurations of solvent and configurations of loaded particles. Nonetheless, care should be taken when comparing to open tube results, given that the interactions at the pore mouths between bulk and loaded water molecules are neglected. The latter has a stronger effect on the (5,5) pore, as shown in the cumulative transfer free energies (see Fig. 3). On the other hand, $\langle E^{C}_{\mathrm{WF-WF}}\rangle$ builds-up progressively, in a non-linear fashion showing a cooperative effect. Again the discontinuity at the last points are due to periodicity. The consistently positive values for $\langle E^{\mathrm{VdW}}_{\mathrm{WF-WF}}\rangle$ are a reflection of the tightly packed water chain within the pore, which becomes more pronounced at higher loads where the dipole–dipole terms overcome dispersion interactions. $\langle E_{\mathrm{WF-WF}}\rangle$ should be explicitly included in any reduced description; recently developed 1D Ising models add these terms in the form of dipole–dipole and (hydrogen-bonded) contact energies.[26] The aforementioned analysis serves to explain the lower values of $\Delta E^{(5,5)}_{(n+1)\rightarrow(n)}$ from Table 1; as seen in Fig. 4, $\langle E^{C}_{\mathrm{WF-WF}}\rangle$ is systematically lower than its (6,6) counterpart. Interestingly the confinement has stronger effects on the electrostatic interactions of the water file than on the chain–tube interaction, the values of which do not greatly differ between the pores.

3.3.2 Hydrogen bonds and dipolar alignment. To explore periodicity effects and gain more insight into the nature of the transfer energies presented in Table 1, water dipolar alignment and hydrogen bonds per water molecule were investigated. In Fig. 5 and 6 the average number of hydrogen bonds per water molecule ($\langle$H-bonds/$n\rangle$) and distributions of the cosine between the water dipole (μ) and the pore axis, *i.e.* z-axis (cos(θ)), for each loading state are depicted. In both (5,5) and (6,6) systems, $\langle$H-bonds/$n\rangle$ monotonically increases, and the big jumps observed at specific loadings, *e.g.* n = 11 for the (5,5) and n = 12, are due to periodicity, as an extra H-bond is formed between a donor at one end of the tube and acceptor at the other. Not surprisingly, this correlates with the energy jumps at those loading states (see Table 1 and Fig. 4). The lower values for ($\langle$H-bonds/$n\rangle$) in the (5,5) pore are a consequence of the geometric confinement experienced by the particles, which on average hinder the hydrogen bond interactions as there is less space to form the adequate angle between donor and acceptor groups (see Fig. 2). It is well known that a strong dipolar alignment is present in single file water. In Fig. 6 normalized histograms for cos(θ) are shown for both systems. Regarding fully loaded tubes (n > 10), only one state for cos(θ) occurs with very narrow peaks around −1, reflecting a strong dependence on the initial conditions, a clear consequence of the high energetic cost of switching μ. As anticipated, both systems switch toward a bimodal mode with peaks at −1 and 1 when water molecules are sequentially removed. The peaks become wider with lower water loadings. Interestingly, even for n = 2, the bimodal mode is still displayed. The (5,5) system presents, in general, more symmetric distributions, a case for a system that shows fewer correlations *i.e.* the energetic interactions are weaker, see Table 1 and Fig. 4. At n = 1, the distributions are uniform due to the lack of dipole–dipole interactions that induce the alignment. Essentially, these results are in line with those of open non-periodic tubes (for more details see Fig. S5, ESI†).

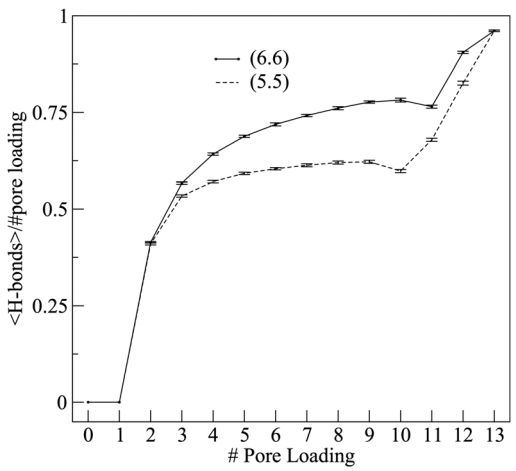

Fig. 5 Average number of hydrogen bonds per water molecule as a function of the loading state for the (5,5) and (6,6) systems.

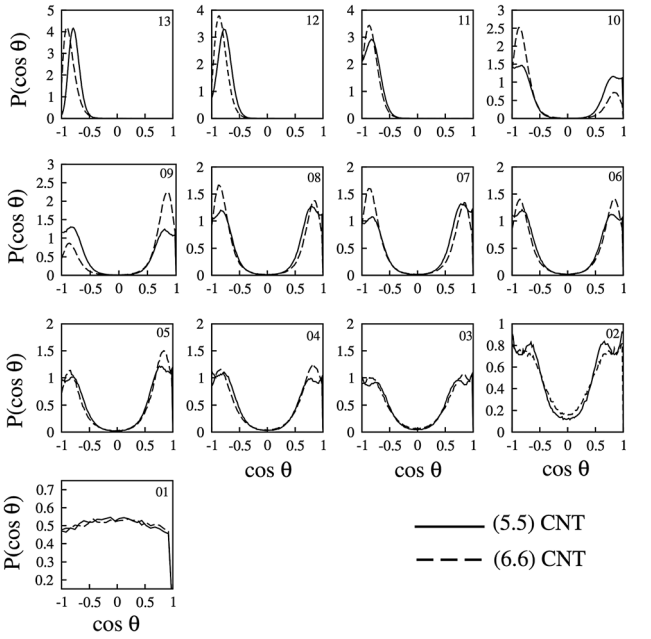

Fig. 6 Distributions of cos(θ) at each loading state, for the (6,6) and (5,5) systems. θ is the angle between the water dipole μ and the z-axis.

3.4 Transfer entropies

The (6,6) single-walled CNT has been extensively described in the literature, particularly in MD studies,[7,20–23] allowing for a detailed comparison of our results with previous work. The (6,6) pore initial loading states are clearly entropically favored, as shown by the negative entropies of transfer to the bulk (see the last rows of columns 4 and 5 of Table 1). Interestingly $T\Delta S^{(6,6)}_{(1)\rightarrow(0)}$ = −21.2 kJ mol^{-1} is almost equivalent to the water entropy of solvation ($T\Delta S_{\mathrm{solv}}$ = −19.0 kJ mol^{-1}), which implies that a single water molecule within the tube is practically in the

gas-phase condition without fully losing its energetic interactions, rendering $\Delta A^{(6,6)}_{(1)\rightarrow(0)}$ close to zero. Other authors have described this phenomenon in terms of liquid to gas-phase transitions.[43] Compared to previous studies, $T\Delta S^{(6,6)}_{(1)\rightarrow(0)}$ agrees with data reported by Vaitheeswaran and collaborators[21] (-15.9 kJ mol^{-1}) but differs significantly from the more recent values by Waghe *et al.* (-0.6 kJ mol^{-1}).[22] Even though the same authors have found that $T\Delta S$ is rather insensitive to the parameter set employed,[21,22] the latter was computed for an open non-periodic tube, thus reflecting the strong coupling of this single water molecule to the bulk phase, which will certainly reduce its entropy. On the other hand, $T\Delta S^{(6,6)}_{(1)\rightarrow(0)}$ is strikingly similar to $T\Delta S_{\mathrm{solv}} = -21.2$ kJ mol^{-1} of Olano *et al.* reported for TIP3P from the hydrophobic cavity of the protein barnase,[28] suggesting that similar entropic effects are a more general feature of hydrophobic cavities. Up to $n = 10$, *i.e.* 84% of loading, $T\Delta S^{(6,6)}_{(n+1)\rightarrow(n)}$ are still favorable but practically zero, implying that, notwithstanding the confinement, there is an intrinsic contribution from translations and rotations equivalent to the bulk phase; similar trends are reported up to 57% and 66% of loading, for shorter periodic and non-periodic tubes respectively.[21,22] Further loadings, up to 90%, dramatically shift towards positive transfer entropies, which is expected due to the smaller available volume, consequently reducing the translational degrees of freedom; besides, rotations along the tube axis become extremely correlated (see below). It seems that at these loading stages, periodicity has no noticeable effects given the overall qualitative agreement between our results (see first two rows of columns 4 and of Table 1) and previously reported data.[21,22] One final point is the negative bulk transfer entropies observed for the average loading of the (6,6) system ($n \simeq 11$, see Table 1). These can be compared to the entropies calculated by Pascal *et al.*[23] which for infinite tubes were filled with the average loading of open tubes. Even though their reported value is on the order of 12 kJ mol^{-1}, qualitatively it is striking and counterintuitive to observe that even for almost fully loaded states, entropy favors the confined state.

Regarding the (5,5) transfer entropies, thermodynamic data are scarcely available and to our knowledge few have employed them in simulation studies. Nonetheless, Hummer and coworkers[7,21,22] have utilized (6,6) pores with modified Lennard-Jones parameters, effectively reducing the pore diameter, thus permitting a qualitative comparison. A similar trend is observed with respect to the (6,6) case, with initial loading states being entropy driven and small transfer bulk entropies of up to 90% of loading. There is an increment of $T\Delta S^{(5,5)}_{(1)\rightarrow(0)}$ of around 5 kJ mol^{-1}, which is expected due to the reduced pore size, which causes frictional effects on the moving particles. Similarly, at a loading of 90% and above, $T\Delta S^{(5,5)}_{(n+1)\rightarrow(n)}$ is in line with the (6,6) system and previous data[21,22] suggesting that both periodicity and the particular pore geometry do not substantially affect those. The higher values of $T\Delta S^{(5,5)}_{(n+1)\rightarrow(n)}$, for $n > 11$, are expected as these are overloaded states which were not observed in simulations of open (5,5) tubes.

3.4.1 Diffusivity and reorientational correlation times. A more profound understanding of the calculated transfer entropies can be gained by studying dynamical properties such as diffusivity and rotational relaxation times. In Table 2 water self-diffusion constants along the tube axis (D_z) for different pore loadings of the (6,6) and (5,5) systems employing eqn (23) are presented.

Table 2 Diffusion constant along the pore axis

	System (6,6)	System (5,5)
# Pore loading	D_z [nm^2 ps^{-1}]	D_z [nm^2 ps^{-1}]
4	—	0.172
3	0.290	0.095
2	0.427	0.156
1	1.535	0.160

Bulk SPC D_{xyz} [nm^2 ps^{-1}] = 0.0041. All values were computed at 298 K.

Before discussing these results, the validity of eqn (23) needs to be addressed; previous authors have shown that the Einstein relation no longer holds for water in non-homogeneous media, particularly for confined states. Consequently, several corrections and formulations have been derived;[44,45] other authors predict unidirectional normal diffusion at longer time-scales for open tubes.[46] In the case of fully loaded periodic tubes, we observed highly correlated motion; moreover, the water file flows as a single particle along the pore axis, which renders constant unidirectional velocities (see Fig. S6 and S7 and Table S2, ESI†). Thus the mean-square displacement (MSD) becomes quadratic in time indicating ballistic diffusion. This phenomenon has previously been reported for infinite (8,8) pores.[47] The ballistic diffusion was observed down to 30% loading; below these the concerted movement no longer happens, switching towards a Fickian regime. In Table 2 we show only the results for these loadings; for the complete set of MSD calculations we refer to Fig. S6 and S7 (ESI†). For both pores, D_z remains 2 orders of magnitude larger than bulk water. This is expected due to the frictionless nature of the flow within the tube and suggests that at low pore loadings, enclosed water is translationally entropically favored compared to the bulk. Moreover, D_z in the (5,5) system is always lower due to confinement, which is in agreement with the lower transfer entropies to the bulk shown in Table 1. Other authors have shown a similar trend in terms of translational degrees of freedom in the form of distributions of nearest–neighbor particles.[21]

Reorientational relaxation times of the dipole μ (τ^{μ}) and H–H ($\tau^{\mathrm{H-H}}$) vectors calculated using eqn (21) and (22) are shown in Table 3. In the case of the perfect dipolar alignment, these vectors represent rotations along the pore axis and perpendicular to it. The confinement in the tube generates a strong anisotropy between τ^{μ} and $\tau^{\mathrm{H-H}}$. The former is highly sensitive to the pore loading, having relaxation times on the order of tens of nanoseconds, a clear indication of the strong correlations between the dipoles. Moreover, at full loadings ($n > 10$), not even a single dipole flipping event was recorded in 100 ns (see Fig. 6), preventing the calculation of τ^{μ}. As expected, the (6,6) system always displays bigger values for τ^{μ} at loadings of over 40%. Below this threshold the dipolar coupling is not as strong and similar values for τ^{μ} for the (6,6) and (5,5) systems are obtained. In contrast, the lower values for $\tau^{\mathrm{H-H}}$ indicate fast rotations around the pore axis, and the constant exchange

Table 3 Reorientational relaxation times for the μ (τ^{μ}) and H–H (τ^{H-H}) vectors

	System (6,6)		System (5,5)	
# Pore loading	τ^{μ} [ps]	τ^{H-H} [ps]	τ^{μ} [ps]	τ^{H-H} [ps]
13	—	3.13	—	7.22
12	—	0.89	—	0.50
11	—	0.27	—	0.12
10	12×10^{4} [a]	0.49	9.6×10^{3} [a]	0.12
9	18×10^{4} [a]	0.55	5.9×10^{2} [a]	0.15
8	5.6×10^{2} [a]	0.61	3.5×10^{2} [a]	0.15
7	2.0×10^{3} [a]	0.58	2.7×10^{2} [a]	0.16
6	6.4×10^{2} [a]	0.61	2.7×10^{2} [a]	0.17
5	2.1×10^{2} [a]	0.54	1.5×10^{2} [a]	0.20
4	46	0.85	48	0.28
3	13	1.57	14	0.58
2	3.18	2.00	2.00	1.28
1	0.05	0.06	0.05	0.05

All values were computed at 298 K. Calculations performed over 1 ns MD simulation with configurations stored every 10 fs. Bulk SPC: τ^{μ} [ps] = 3.20, τ^{H-H} [ps] = 2.90. [a] 100 ns MD employed.

between the dangling hydrogen of neighbor molecules explains these unusually fast rotations.[25] τ^{H-H} tends to be independent of the loading; however at very low loadings, $n < 4$ converges towards bulk values. Both τ^{μ} and τ^{H-H} at $n = 1$, are very low, a clear indication of the lack of correlations normally present in the gas phase. Note the similarity of all τ-values between a pore loading of 2 and bulk water.

4 Conclusions

The thermodynamics of water loading of periodic (6,6) and (5,5) single-walled carbon nanotubes was extensively studied employing free energy calculations for both systems. The (6,6) results are in line with previous results[7,21,22] as well as with PMF calculations of an open pore displaying very favorable free energies towards the loading states which are both entropically and energetically driven. The (5,5) systems, in contrast, do not favor loaded states and appear more sensitive to the bulk pressure. It was found that entropic contributions dominate the initial loading states, whereas energetic contributions systematically build up for higher loadings. For the former, increased rotation and translation are the main contributors.

Diffusivity for low loading states are 2 to 3 orders of magnitude higher than for the bulk and at high loading states becomes ballistic as the water file moves as a single entity. Rotations show a high degree of anisotropy; rotations of the dipole axis are very rare, with increased frequency for lower pore loadings. Perpendicular rotations along the pore axis are enhanced and almost independent of the loadings, compensating for the entropy loss due to confinement, which in part explains the mostly negligible transfer entropies for the majority of the loading states.

In terms of energetics, at high loading states, electrostatics plays the main role reflected in hydrogen bonds and dipolar alignment. These are further enhanced by periodicity, even though entropy plays a role. The main difference between the (6,6) and (5,5) systems are the electrostatic interactions, which for the (5,5) tubes are greatly reduced due to the geometric constraints imposed by the smaller pore size of these tubes.

Acknowledgements

Financial support from the Fondo Nacional de Desarrollo Científico y Tecnológico (FONDECYT) project number 3130547, Programa de Financiamiento Basal PFB16 Fundación Ciencia para la Vida, project ACT-1107 PIA-CONICYT, ICM-ECONOMIA P09-022-F, Vienna Science and Technology Fund (WWTF) grant number LS08-QM03, and the European Research Council (ERC) grant number 260408 is gratefully acknowledged.

References

1 A. Alexiadis and S. Kassinos, *Chem. Rev.*, 2008, **108**, 5014.
2 E. Snow, F. Perkins, E. Houser, S. Badescu and T. Reinecke, *Science*, 2005, **307**, 1942–1945.
3 B. Hinds, N. Chopra, T. Rantell, R. Andrews, V. Gavalas and L. Bachas, *Science*, 2004, **303**, 62–65.
4 R. Singh, D. Pantarotto, L. Lacerda, G. Pastorin, C. Klumpp, M. Prato, A. Bianco and K. Kostarelos, *Proc. Natl. Acad. Sci. U. S. A.*, 2006, **103**, 3357–3362.
5 J. Garate, N. English and J. MacElroy, *J. Chem. Phys.*, 2011, **134**, 055110.
6 M. Gordillo and J. Mart, *Chem. Phys. Lett.*, 2000, **329**, 341–345.
7 G. Hummer, J. Rasaiah and J. Noworyta, *Nature*, 2001, **414**, 188–190.
8 F. Zhu and K. Schulten, *Biophys. J.*, 2003, **85**, 236–244.
9 J. C. Rasaiah, S. Garde and G. Hummer, *Annu. Rev. Phys. Chem.*, 2008, **59**, 713–740.
10 J. Garate, N. English and J. MacElroy, *Mol. Simul.*, 2009, **35**, 3–12.
11 J. Garate, N. English and J. MacElroy, *J. Chem. Phys.*, 2009, **131**, 114508.
12 S. Cambr and W. Wenseleers, *Angew. Chem.*, 2011, **50**, 2764–2768.
13 H.-J. Wang, X.-K. Xi, A. Kleinhammes and Y. Wu, *Science*, 2008, **322**, 80–83.
14 N. Naguib, H. Ye, Y. Gogotsi, A. G. Yazicioglu, C. M. Megaridis and M. Yoshimura, *Nano Lett.*, 2004, **4**, 2237–2243.
15 A. Berezhkovskii and G. Hummer, *Phys. Rev. Lett.*, 2002, **89**, 064503.
16 G. Hummer, J. C. Rasaiah and J. P. Noworyta, *Nature*, 2001, **414**, 188–190.
17 A. Kalra, S. Garde and G. Hummer, *Proc. Natl. Acad. Sci. U. S. A.*, 2003, **100**, 10175–10180.
18 J. Li, X. Gong, H. Lu, D. Li, H. Fang and R. Zhou, *Proc. Natl. Acad. Sci. U. S. A.*, 2007, **104**, 3687–3692.
19 X. Gong, J. Li, H. Lu, R. Wan, J. Li, J. Hu and H. Fang, *Nat. Nanotechnol.*, 2007, **2**, 709–712.
20 C. Won, S. Joseph and N. Aluru, *J. Chem. Phys.*, 2006, **125**, 114701.

21 S. Vaitheeswaran, J. C. Rasaiah and G. Hummer, *J. Chem. Phys.*, 2004, **121**, 7955–7965.
22 A. Waghe, J. C. Rasaiah and G. Hummer, *J. Chem. Phys.*, 2012, **137**, 044709.
23 T. A. Pascal, W. A. Goddard and Y. Jung, *Proc. Natl. Acad. Sci. U. S. A.*, 2011, **108**, 11794–11798.
24 J. Köfinger, G. Hummer and C. Dellago, *J. Chem. Phys.*, 2009, **130**, 154110.
25 J. Köfinger, G. Hummer and C. Dellago, *Phys. Chem. Chem. Phys.*, 2011, **13**, 15403–15417.
26 J. Köfinger, G. Hummer and C. Dellago, *J. Chem. Phys.*, 2009, **130**, 154110.
27 L. Maibaum and D. Chandler, *J. Phys. Chem. B*, 2003, **107**, 1189–1193.
28 L. R. Olano and S. W. Rick, *J. Am. Chem. Soc.*, 2004, **126**, 7991–8000.
29 M. Christen, P. H. Hünenberger, D. Bakowies, R. Baron, R. Bürgi, D. P. Geerke, T. N. Heinz, M. A. Kastenholz, V. Kräutler, C. Oostenbrink, C. Peter, D. Trzesniak and W. F. van Gunsteren, *J. Comput. Chem.*, 2005, **26**, 1719–1751.
30 T. C. Beutler, A. E. Mark, R. C. van Schaik, P. R. Gerber and W. F. van Gunsteren, *Chem. Phys. Lett.*, 1994, **222**, 529–539.
31 R. W. Zwanzig, *J. Chem. Phys.*, 1954, **22**, 1420–1426.
32 B. Lai and C. Oostenbrink, *Theor. Chem. Acc.*, 2012, **131**, 1–13.
33 M. Allen and D. Tildesley, *Computer Simulations of Liquids*, Oxford Science Publications, 1987.
34 N. Schmid, C. D. Christ, M. Christen, A. P. Eichenberger and W. F. van Gunsteren, *Comput. Phys. Commun.*, 2012, **183**, 890–903.
35 S. Riniker, C. D. Christ, H. S. Hansen, P. H. Hünenberger, C. Oostenbrink, D. Steiner and W. F. van Gunsteren, *J. Phys. Chem. B*, 2011, **115**, 13570–13577.
36 J.-P. Ryckaert, G. Ciccotti and H. J. C. Berendsen, *J. Comput. Phys.*, 1977, **23**, 327.
37 R. W. Hockney, *Methods Comput. Phys.*, 1977, **9**, 136–211.
38 I. G. Tironi, R. Sperb, P. E. Smith and W. F. van Gunsteren, *J. Chem. Phys.*, 1995, **102**, 5451–5459.
39 R. D. Lins and P. H. Hünenberger, *J. Comput. Chem.*, 2005, **26**, 1400–1412.
40 S. Nosé, *J. Chem. Phys.*, 1984, **81**, 511–519.
41 W. G. Hoover, *Phys. Rev. A: At., Mol., Opt. Phys.*, 1985, **31**, 1695–1697.
42 A. de Ruiter, S. Boresch and C. Oostenbrink, *J. Comput. Chem.*, 2013, **34**, 1024–1034.
43 O. Beckstein and M. S. P. Sansom, *Proc. Natl. Acad. Sci. U. S. A.*, 2003, **100**, 7063–7068.
44 P. Liu, E. Harder and B. J. Berne, *J. Phys. Chem. B*, 2004, **108**, 6595–6602.
45 A. A. Milischuk and B. M. Ladanyi, *J. Chem. Phys.*, 2011, **135**, 174709.
46 B. Mukherjee, P. K. Maiti, C. Dasgupta and A. K. Sood, *J. Chem. Phys.*, 2007, **126**, 124704.
47 A. Striolo, *Nano Lett.*, 2006, **6**, 633–639.

